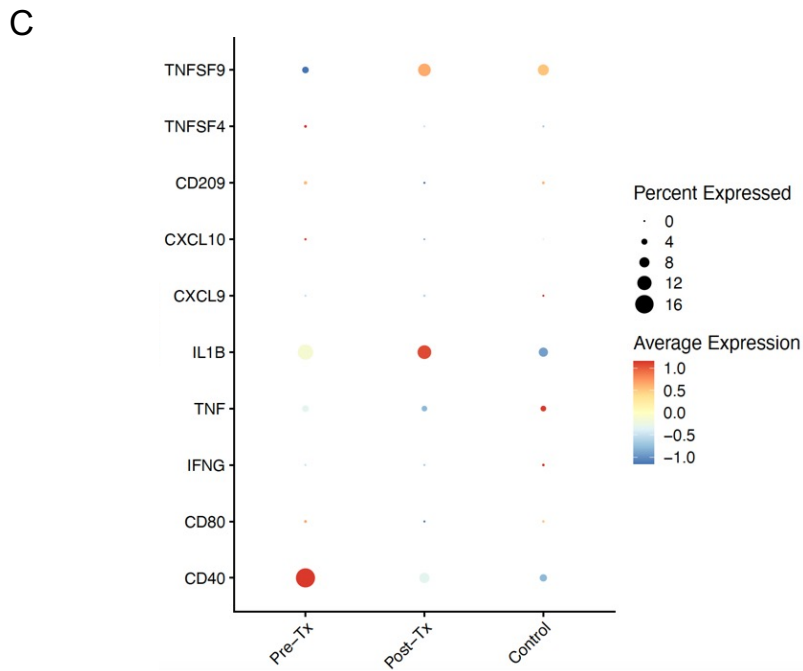
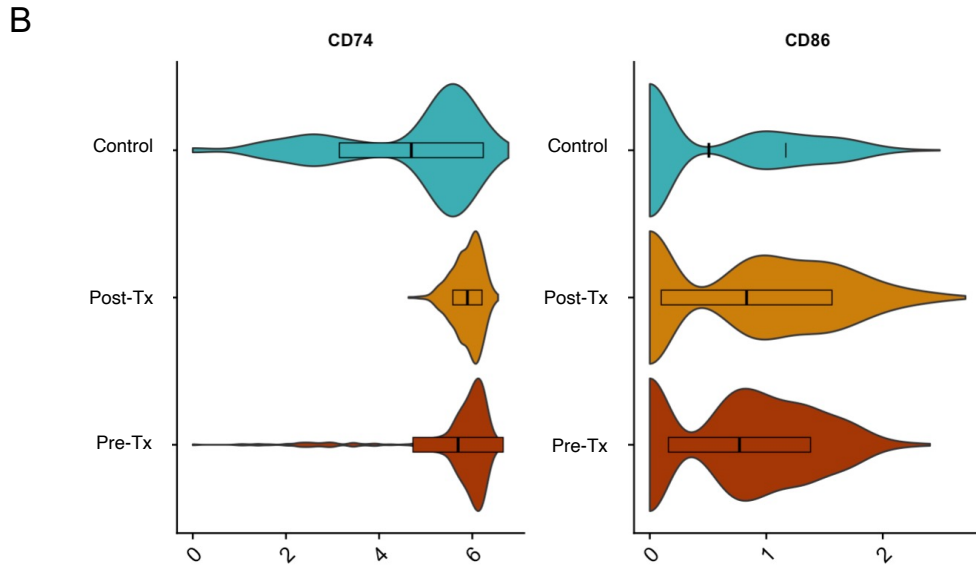
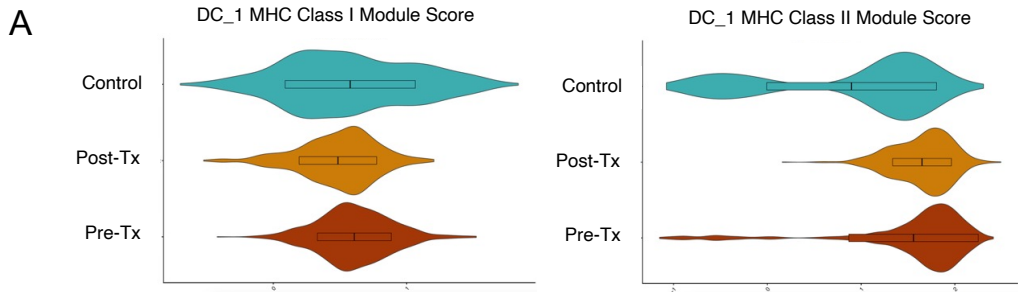


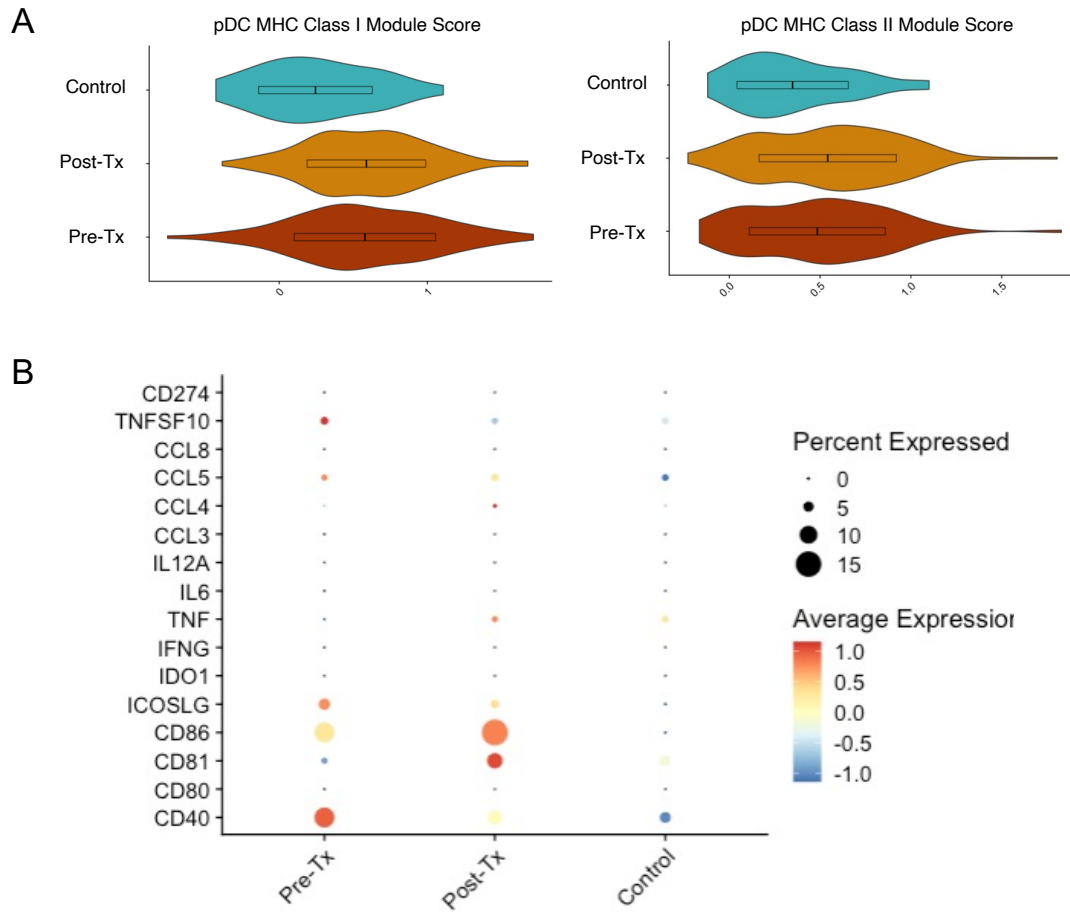
Supplemental Figure 1. Cluster frequency changes in the CSF.

Per sample cluster frequencies in baseline MS patients with paired follow up samples (n=5) and healthy donors (n=6)



Supplemental Figure 2. Transcriptomic characterization of CSF DC_1 cluster.

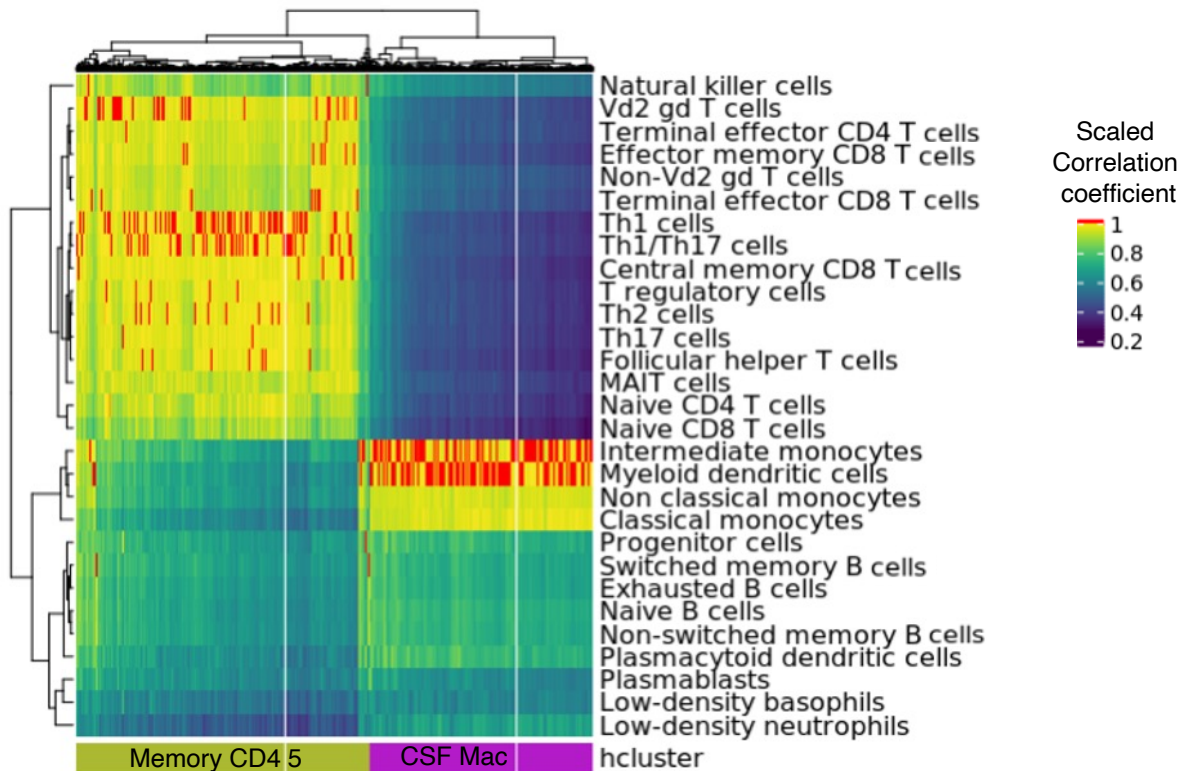
(A) MHC class I and class II gene module scores in healthy, pre- and post- treatment CSF samples. **(B)** CD74 and CD86 gene expression in healthy, pre- and post- treatment CSF samples. **(C)** Expression level and percent of expression of inflammatory dendritic cell genes.



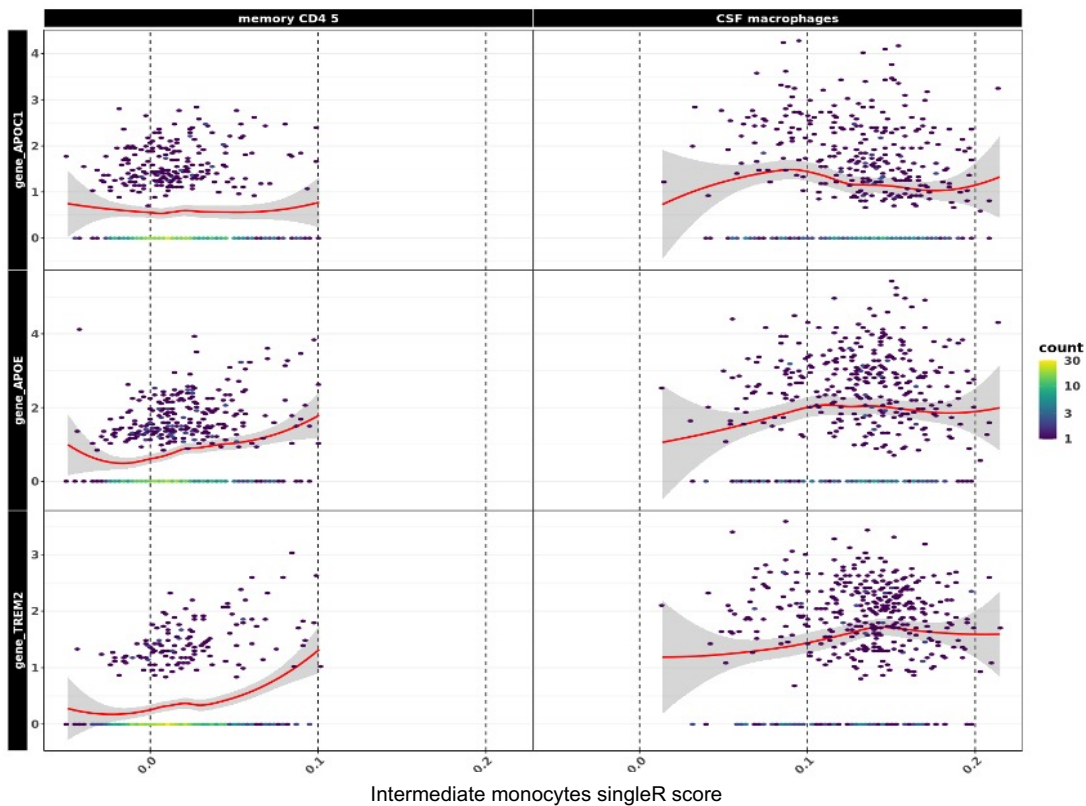
Supplemental Figure 3. Transcriptomic characterization of CSF pDC cluster.

(A) MHC class I and class II gene module scores in healthy, pre- and post- treatment CSF samples. **(B)** Individual gene expression in healthy, pre- and post- treatment CSF samples.

A

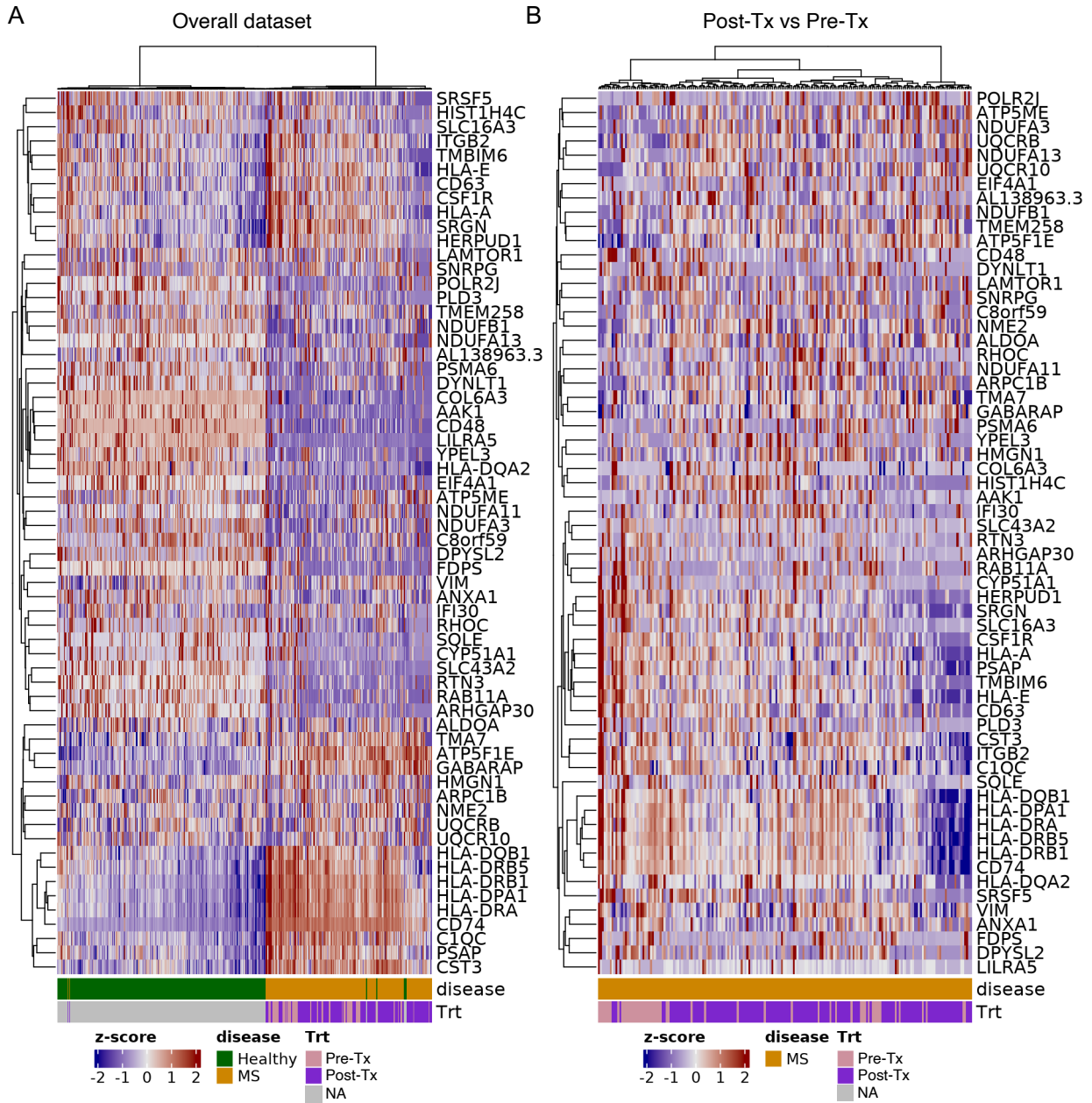


B



Supplemental Figure 4. Common CSF signature between macrophage and T cell clusters.

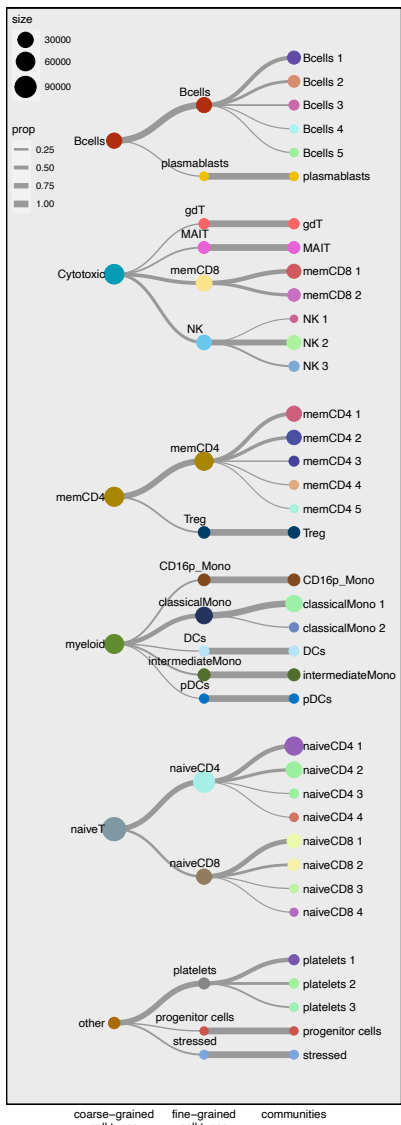
(A) Community based clustering (Louvain) on shared nearest neighbor graph led to a cluster with mixed lineages (T cells and myeloid cells), based on singleR scoring against the Monaco reference. Separation of the two lineages by hierarchical clustering let us define two clusters for downstream analysis. **(B)** 'Intermediate monocytes' singleR score separates each lineage, but both lineages express similar gene signature associated with CSF residency (*APOC1*, *APOE*, *TREM2*).



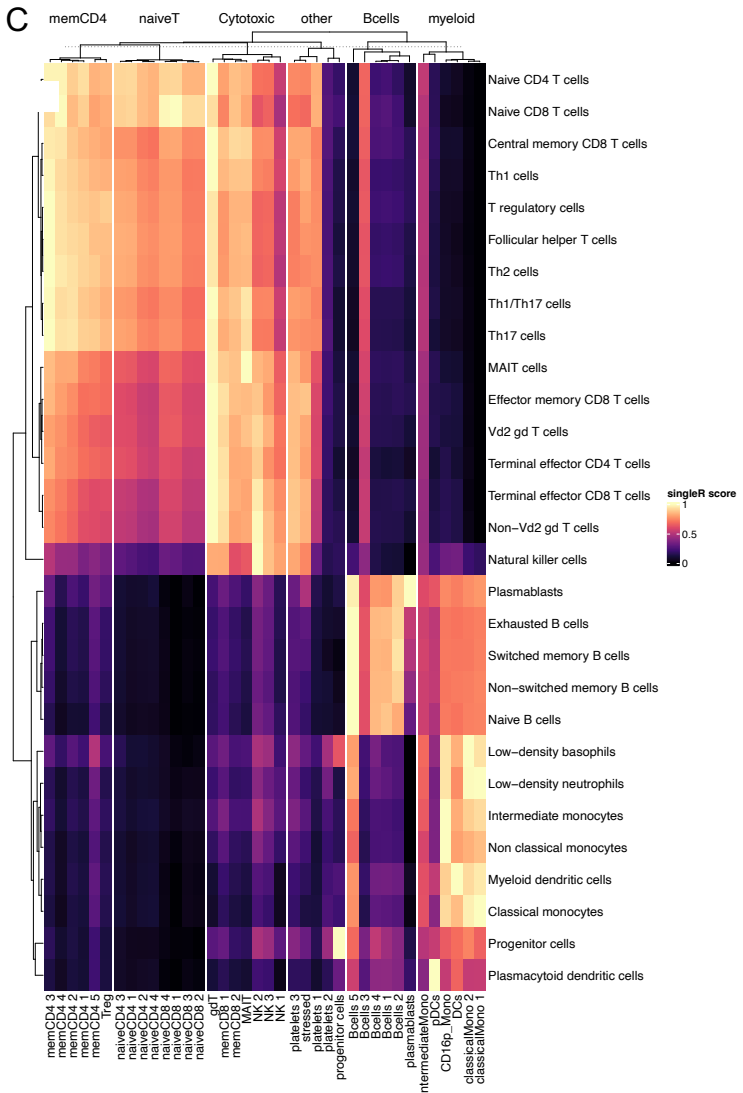
Supplemental Figure 5. Transcriptomic changes in CSF macrophages.

(A and B) Heatmap of differentially expressed genes in the 'Mac 1' CSF macrophage cluster for MS baseline vs healthy donor (A) and MS follow up vs baseline (B).

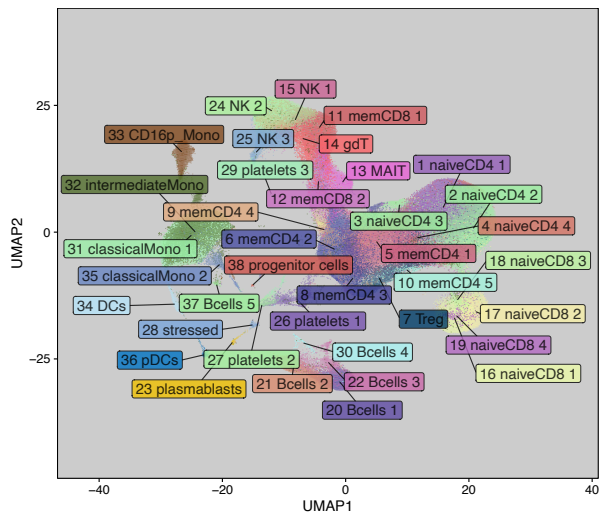
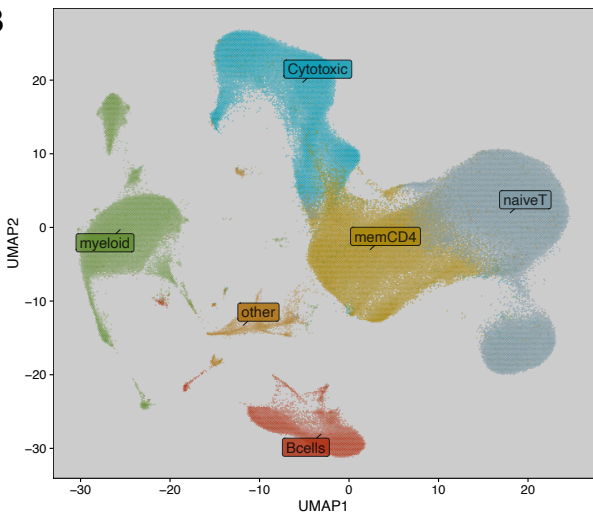
A



C

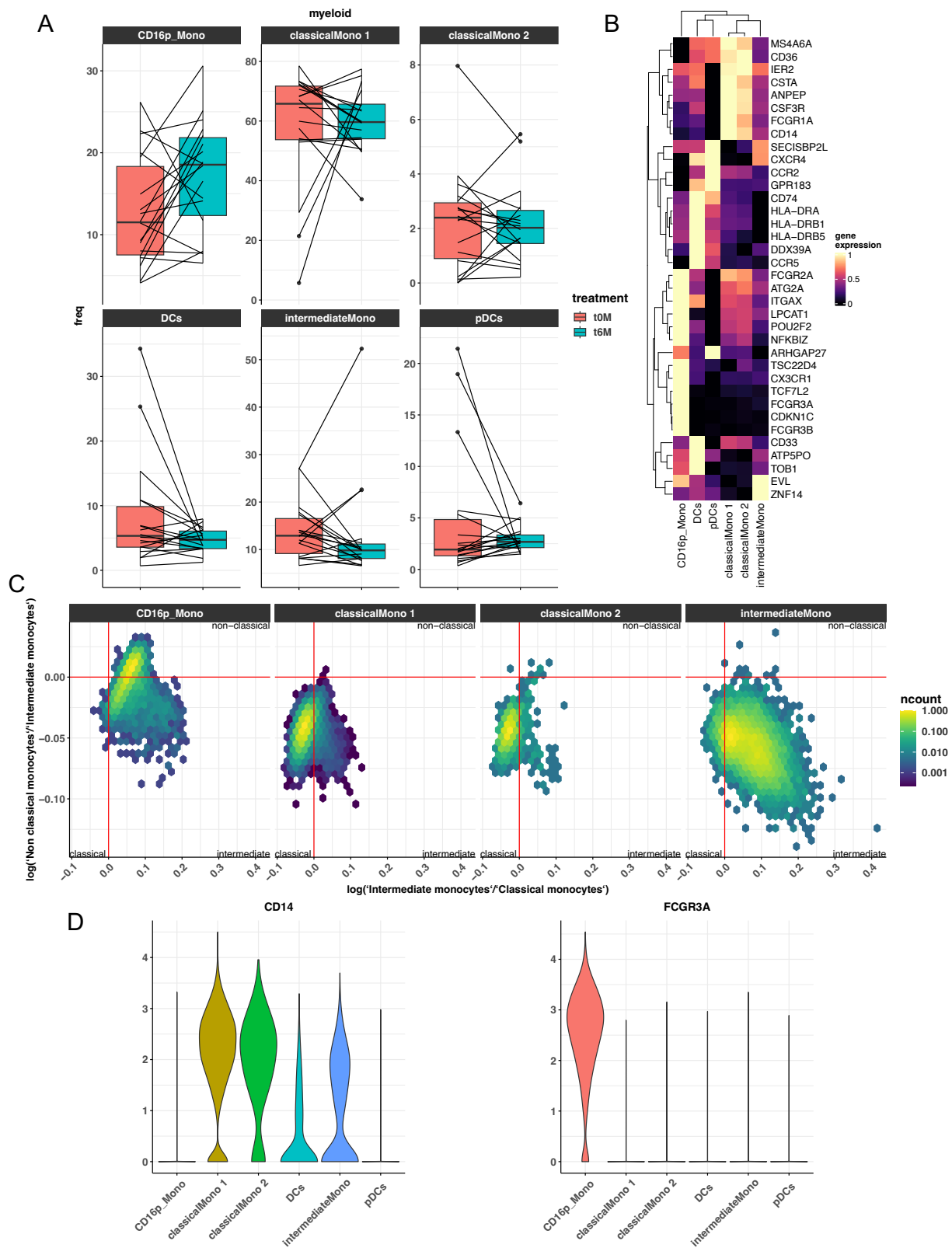


B



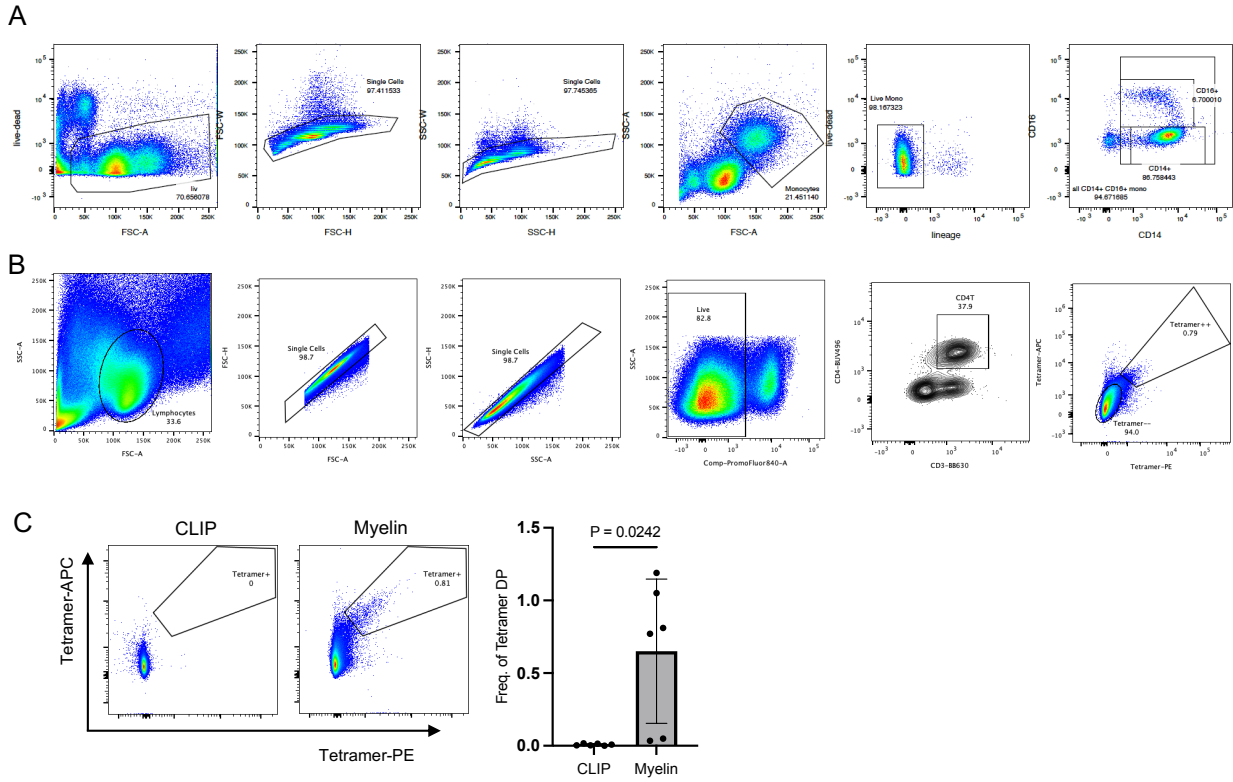
Supplemental Figure 6. Community detection and aggregation of PBMC scRNAseq dataset.

(A) initial community detection resolution (coarse-grained cell type) and subsequent nested community detection (community). Communities were then merged into fine-grained cell types. **(B)** UMAP embedding annotated with coarse-grained cell types assignments and communities assignments. **(C)** singleR scores heatmap for fined-grained cell types, grouped by coarse-grained cell types.

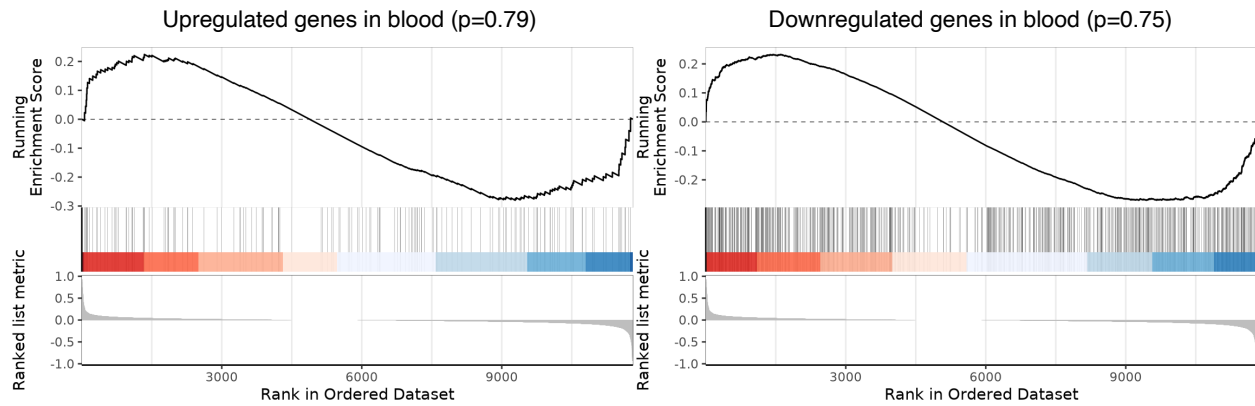


Supplemental Figure 7. Characterization of myeloid clusters in PBMC dataset.

(A) frequency changes in myeloid clusters in MS follow up vs baseline samples. **(B)** heatmap of myeloid cell type gene markers across fine-grained cell types. **(C)** singleR monocytes subtypes score comparison across clusters defines 3 quadrants to differentiate between classical, intermediate, and non-classical subsets. CD16+ monocytes cluster presents with a mixture of intermediate and non-classical cells. **(D)** RNA expression of CD14 and FCGR3A (encoding CD16) in myeloid clusters.

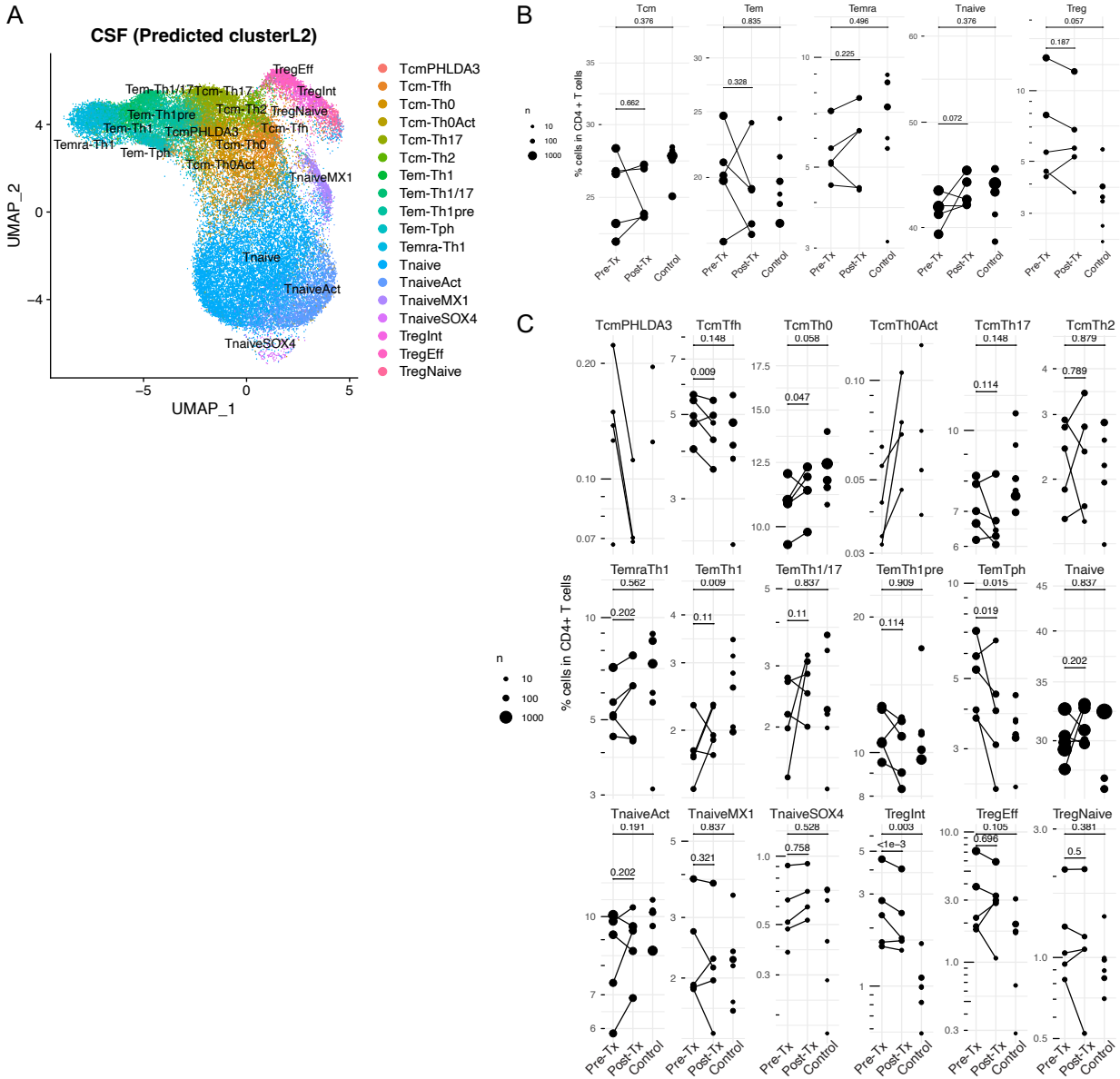


Supplemental Figure 8. Flow cytometry gating strategy and establishment of control. (A and B) Flow cytometry images showed the gating strategy for monocytes (A) and lymphocytes (B). (C) As a negative control, an MHC tetramer loaded with peptide of Class II-associated invariant chain peptide (CLIP) was used (n=6).



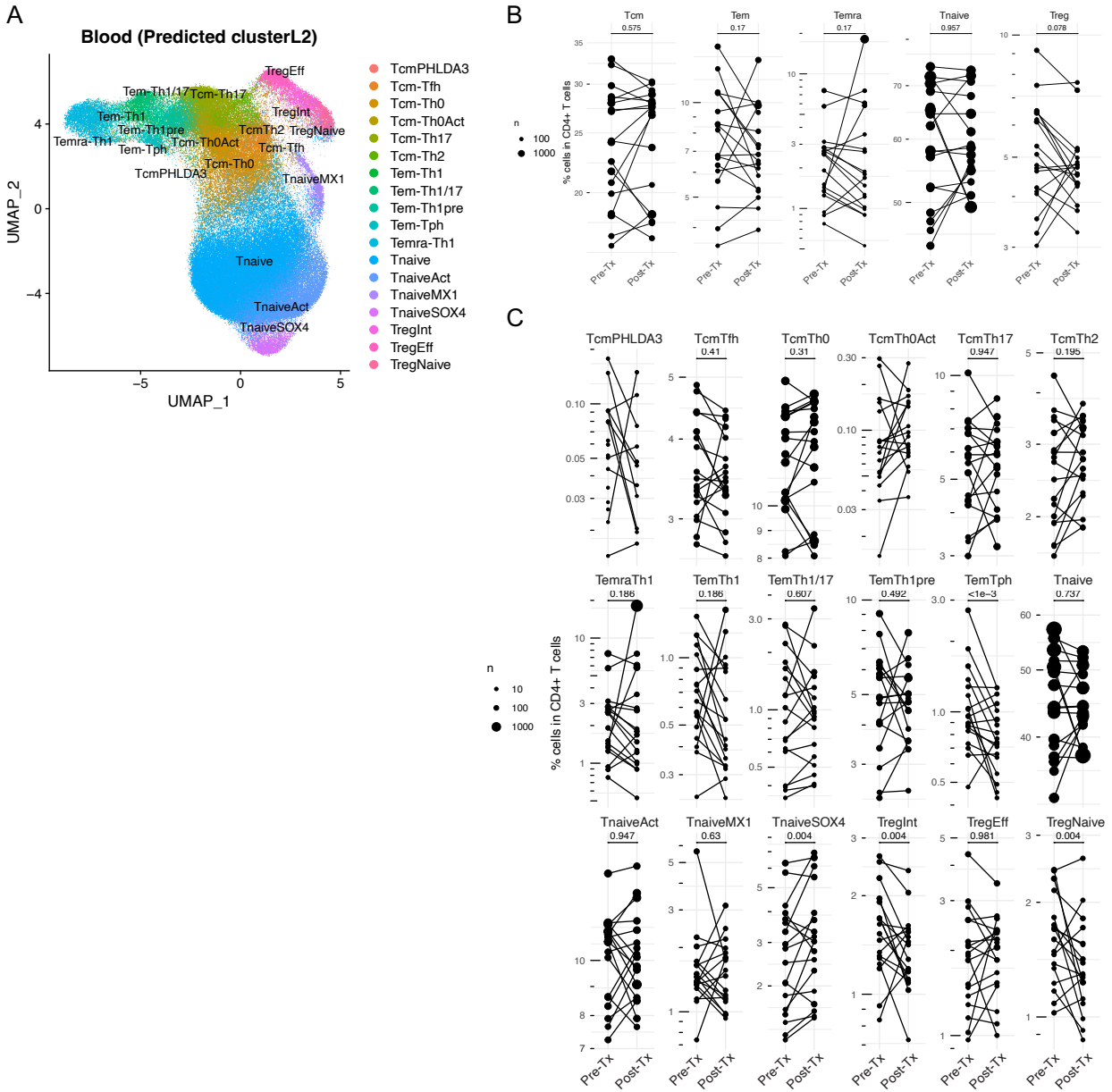
Supplemental Figure 9. GSEA between blood monocytes and CSF macrophages.

GSEA on differential gene expression output from CSF macrophage cluster using custom genesets composed of upregulated and downregulated genes in PBMC cluster 33 of CD16+ monocytes. The absence of significant enrichment suggests distinct dynamics between the two compartments.



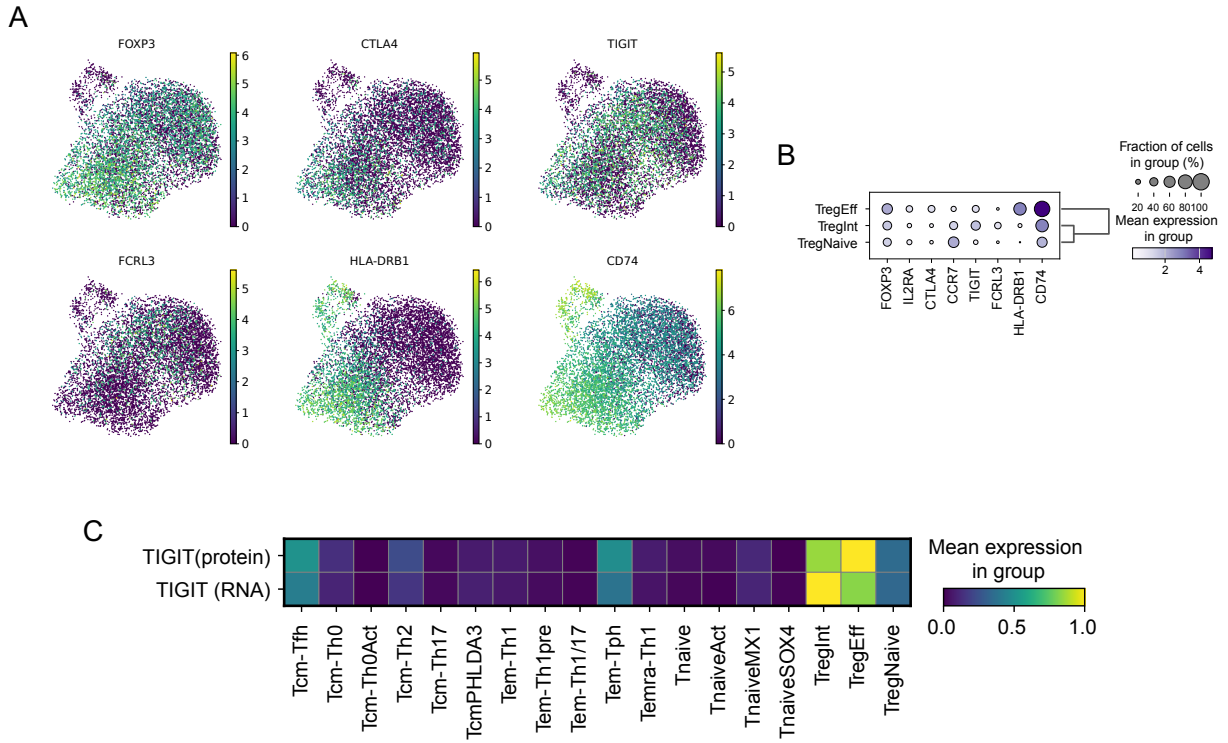
Supplemental Figure 10. CD4+ T cell alterations in CSF

(A) Inferred CSF CD4⁺ T cell clusters on UMAP plot. The clusters were assigned to a detailed cluster (cluster L2) level. **(B and C)** CSF CD4⁺ T cell frequency changes after anti-CD20 treatment in cluster L1 level (B) and cluster L2 level (C). Coefficients of cell frequency change per cluster L2 quantified GLM (method) are visualized on the UMAP plot (left). CD4⁺ T cluster frequency pre- and post-B cell depletion therapy (right).



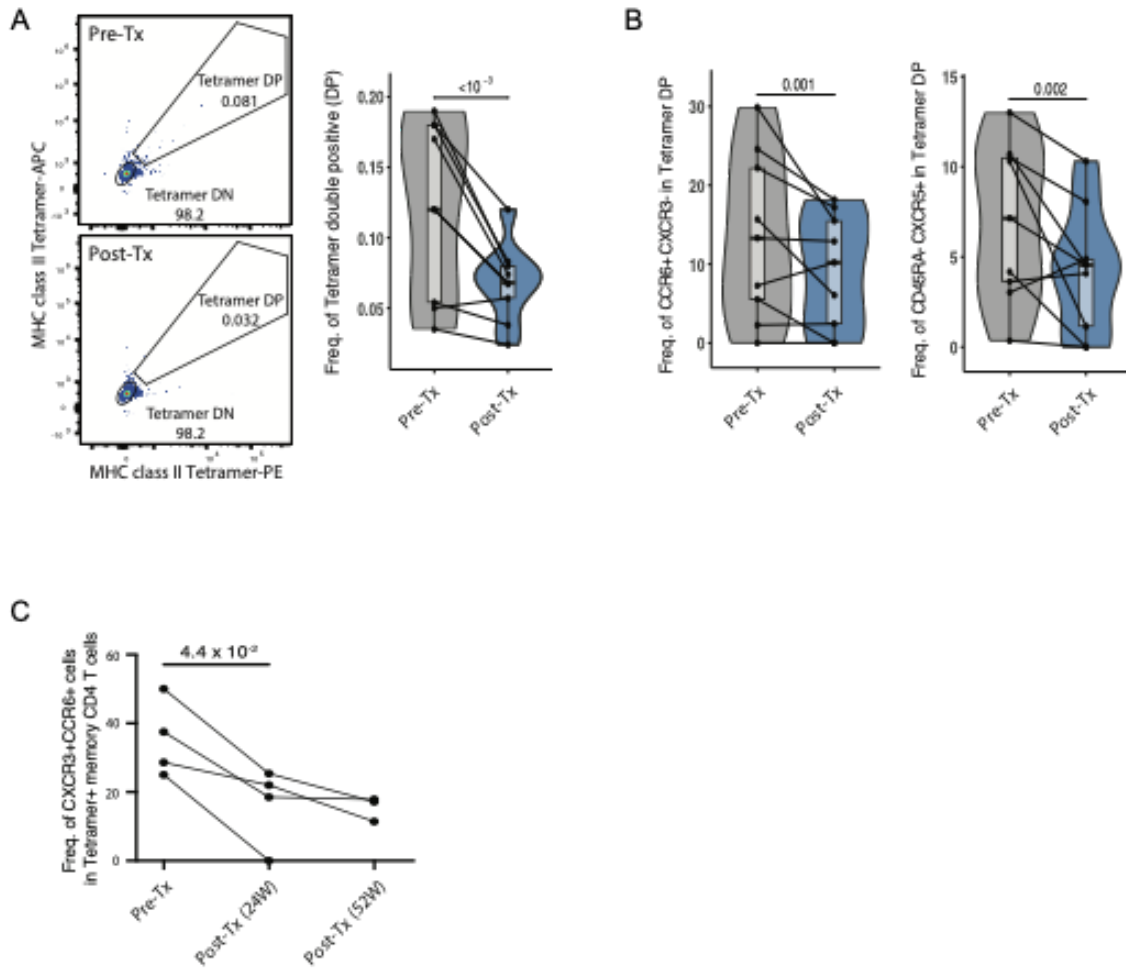
Supplemental Figure 11. CD4⁺ T cell alterations in blood

(A) Inferred blood CD4⁺ T cell clusters on UMAP plot. The clusters were assigned to a detailed cluster (cluster L2) level. **(B and C)** Blood CD4⁺ T cell frequency changes after anti-CD20 treatment in cluster L1 level (B) and cluster L2 level (C). Coefficients of cell frequency change per cluster L2 quantified GLM (method) are visualized on the UMAP plot (left). CD4⁺ T cluster frequency pre- and post-B cell depletion therapy (right).



Supplemental Figure 12. Detailed Treg characteristics

(A and B) Treg marker gene expression. Blood Treg cells were extracted and shown using UMAP (A) or dot plot (B). **(C)** Heatmap showing protein and RNA expression of TIGIT in cluster L2 clusters. CITE-seq data (GSE164378) was used for the visualization.



Supplemental Figure 13. Characteristics of myelin tetramer-reactive T cells in different cohorts.

(A) Flow cytometry analysis of myelin tetramer-reactive CD4+ T cell frequency at pre-treatment and 6-month post-treatment timepoints in different MS cohort (n=9). **(B)** Tfh (CD45RA— CXCR5+) cells in tetramer-reactive CD4+ T cells and Th17 (CCR6+CXCR3-) cells in tetramer-reactive CD4+ T cells frequencies at pre-treatment and 6-month post-treatment timepoints (n=9). **(C)** Longitudinal kinetic analysis of the frequency of autoreactive CCR6+CXCR3+ CD4+ T cells using flow cytometry at pre-treatment (n=4), 24-week post-treatment (n=4) and 52-week post-treatment (n=3) timepoints.